ICESat Full-Waveform Altimetry Compared to Airborne Laser Scanning Altimetry Over The Netherlands

Hieu Duong, *Associate Member, IEEE*, Roderik Lindenbergh, Norbert Pfeifer, and George Vosselman

***Abstract*—Since 2003, the full-waveform laser altimetry system onboard NASA's Ice, Cloud and land Elevation Satellite (ICESat) has acquired a worldwide elevation database. ICESat data are widely applied for change detection of ice sheet mass balance, forest structure estimation, and digital terrain model generation of remote areas. ICESat's measurements will be continued by a follow-up mission. To fully assess the application possibilities of the full-waveform products of these missions, this research analyzes the vertical accuracy of ICESat products over complex terrain with respect to land cover type. For remote areas, validation of individual laser shots is often beyond reach. For a country with extensive geo-infrastructure such as The Netherlands, excellent countrywide validation is possible. Therefore, the ICESat full-waveform product GLA01 and the land elevation product GLA14 are compared to data from the Dutch airborne laser altimetry archive Actual Height model of the Netherlands (AHN). For a total population of 3172 waveforms, differences between ICESat- and AHN-derived terrain heights are determined. The average differences are below 25 cm over bare land and urban areas. Over forests, differences are even smaller but with slightly larger standard deviations of about 60 cm. Moreover, a waveform-based feature height comparison resulted in feature height differences of 1.89 m over forest, 1.48 m over urban areas, and 29 cm over low vegetation. These results, in combination with the presented processing chain and individual waveform examples, show that state-of-the-art ICESat waveform processing is able to analyze waveforms at the individual shot level, particularly outside urban areas.**

***Index Terms*—Actual height model of The Netherlands (AHN), digital terrain models (DTMs), feature height, full waveform, Ice, Cloud and land Elevation Satellite (ICESat), laser altimetry.**

I. Introduction

THE ICE, Cloud and land Elevation Satellite (ICESat) was launched in January 2003 to observe the cryosphere and atmosphere and to measure land topography profiles and canopy heights [1]. These objectives are accomplished using the Geoscience Laser Altimeter System (GLAS), in combination with precise orbit determination (POD) and precise altitude determination (PAD). Since 2003, ICESat has acquired a huge database of raw and processed data organized in 15 data products, i.e., GLA01, . . ., GLA15 [2]. Each product contains a different data type. For example, the GLA01 level-1A product contains the raw full-waveform data, and the GLA14 product provides global land surface elevation data [3].

ICESat data products have been used in many research topics in recent years. Typical applications include forestry (such as estimation of canopy parameters and above-ground biomass [4]–[6], vegetation vertical structure [7]–[9], forest disturbance [10], and single- and two-epoch analyses of ICESat full-waveform data over forested areas [11]) and polar regions, accuracy and precision of digital elevation models (DEMs) [12], [13], mass balance over Antarctica [14], volume change rate of the ice sheet over Greenland [15], snow accumulation on ice sheets [16], and estimation of sea ice thickness by using snow depth on the sea ice [17]. Follow-up missions are planned to continue the acquisition of large footprint waveform data. ICESat-II and the scheduled Deformation, Ecosystem Structure and Dynamics of Ice (DESDynI) mission will also operate a large footprint waveform system.

To obtain insight into ICESat data accuracy, ICESat data were compared and validated by independent data sources. ICESat data were several times compared with data of moderate accuracy, such as InSAR-derived DEMs [18] and Shuttle Radar Topography Mission (SRTM) data [19]–[21]. Elevation differences between ICESat data and SRTM data are discussed either with respect to different land cover types, as derived from Landsat-7 images [21], or over high relief and densely vegetated surfaces [19], [20]. In addition, the highest and lowest elevations derived from the ICESat full-waveform data are also discussed in [19] and [20] to assess the properties of ICESat data over complex land surfaces.

ICESat data are also carefully compared with more accurate data, such as airborne laser scanning data [22]–[24] and Global Positioning System measurements [25]–[27]. According to [25], ICESat-derived elevations are impacted by environmental effects (e.g., forward scattering and surface reflectance) and instrument effects (e.g., pointing biases, detector saturation, and variations in transmitted laser energy). Under ideal conditions, a vertical bias of less than 2 cm with a standard deviation of at least 3 cm is reported [22]–[25].

Manuscript received June 6, 2008; revised February 19, 2009 and April 3, 2009. First published June 23, 2009; current version published September 29, 2009. This work was supported by the Delft Research Centre "Earth."

H. Duong and R. Lindenbergh are with the Delft University of Technology, 2629 HS Delft, The Netherlands (e-mail: v.h.duong@tudelft.nl; r.c.lindenbergh@tudelft.nl)

N. Pfeifer is with the Institute of Photogrammetry and Remote Sensing, Vienna University of Technology, 1040 Vienna, Austria (e-mail: np@ipf.tuwien.ac.at).

G. Vosselman is with the International Institute for Geo-Information Science and Earth Observation (ITC), 7500 AA Enschede, The Netherlands (e-mail: vosselman@itc.nl).

Color versions of one or more of the figures in this paper are available online at http://ieeexplore.ieee.org.

Digital Object Identifier 10.1109/TGRS.2009.2021468

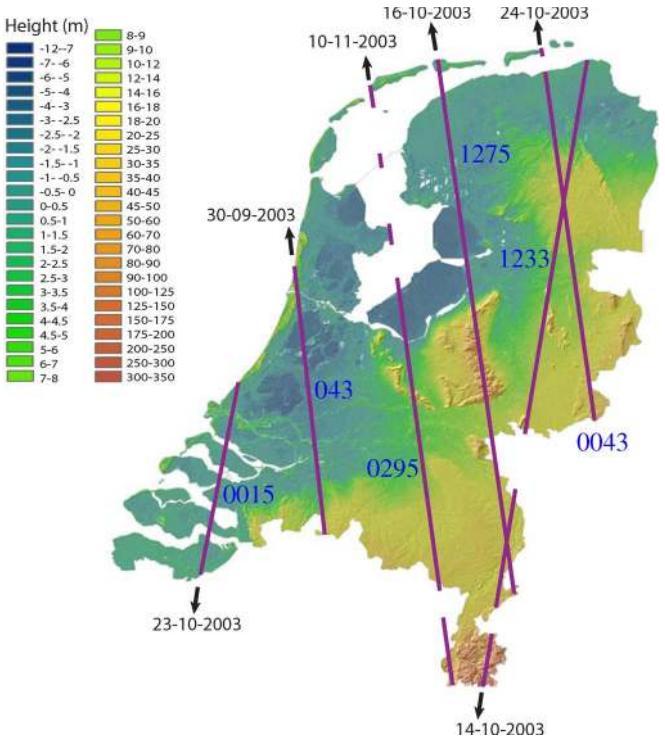

Fig. 1. Study area. Six ICESat ground tracks (magenta) displayed with the AHN. The upward arrows indicate ascending tracks, and the downward arrows descending tracks. ICESat reference track numbers are given in blue.

For validating ICESat elevations, often, terrain is chosen with simple surface characteristics, such as sea ice [22] or the Salar de Uyuni salt flats, Bolivia [25]. Moreover, ICESat elevations, i.e., the GLA06 and GLA12 products, are typically only obtained from the maximum peak of the full waveform. Consequently, the full-waveform data itself and the techniques for processing such data have not thoroughly been investigated. Over land regions, the full-waveform data were only processed and applied for the estimation of forest structure and aboveground biomass [4], [5], [28], canopy cover [7], [8], and forest species inventory [10]. Therefore, in this paper, ICESat elevation (GLA14) data and ICESat full-waveform (GLA01) data are processed and compared with the Dutch national high-accuracy airborne laser scanning product Actual height model of The Netherlands (AHN) for a variety of land cover types.

This research gives clear insight into the accuracies that can be expected over more complex terrain types. To understand the nature of larger differences that occur in the comparison, an analysis of waveforms deviating at the individual shot level was necessary. Such analysis has enabled us to eliminate the most outlying differences.

The objectives of this paper are given as follows: 1) to propose an appropriate way of estimating the accuracy of ICESat data over complex land surfaces containing forests, buildings, and artificial objects; 2) to estimate the accuracy with respect to different land cover classes: forest (broadleaf, mixed and needleleaf), urban, and bare land/low vegetation; and 3) to investigate the choice of waveform parameters suited in comparing the feature heights of forests and buildings.

To do so, a new method of comparison between ICESat and laser scanning data (AHN) is introduced. First, this paper proposes an appropriate method to register the waveform data into a common coordinate system via information provided in the GLA14 product, leading to the so-called georeferenced waveforms. Later on, the most suited position can be extracted from the georeferenced waveform to represent either the surface terrain height or the height of features, such as trees or buildings. On the other side, the many AHN laser points within an ICESat footprint are segmented to obtain one particular segment representing the surface terrain. Moreover, from the AHN laser points, an AHN simulated waveform is created for two reasons: 1) to enable a comparability check between ICESat and AHN waveforms and 2) to enable the extraction of an AHN feature height to be compared with the corresponding ICESat waveform height.

Two comparisons between ICESat data and AHN data are studied in detail in this research, which comprise an accuracy assessment of complex terrain height and a feature height comparison. These comparisons are defined in detail in Section III. The results of the accuracy assessment are evaluated with respect to the different land cover classes according to the CORINE Land Cover 2000 database (CLC2000) [29]. In Section II, study areas and data sets are introduced. Then, the methodology is proposed. Results and future work are discussed at the end of this paper.

II. Study Area and Data

A. Study Area

The area of study is The Netherlands, which is approximately bounded by 3° E to 7° E longitude and 50° N to 54° N latitude, which contains a large variety of land cover types. The total length of the six considered ICESat ground tracks is about 1290 km. Fig. 1 shows a map of the DEM (AHN) of The Netherlands, which is colored by height, together with the six tracks. In this paper, we differentiate results with respect to land cover type. For this purpose, the CLC2000 data set is used.

B. ICESat/GLAS

The GLA01 full-waveform data are, in general, sampled as relative intensities in 200 bins for sea ice and ocean, and 544 bins over land and ice sheets. The bin size is 1 ns. The surface type is determined by the instrument from the onboard DEM.

The GLA14 global land surface elevations are obtained by combining POD [30], PAD [31], and range data. The range data are determined from a time stamp pair corresponding to the centroid of the transmitted pulse and the reference point (mostly the centroid) of the return waveform. After all instrumental, atmospherical, and tidal corrections have been applied [2], geolocated latitude, longitude, and footprint elevation are computed [32]. The position of the reference point is stored as a range offset in GLA14. For coping with the potential complexities of land returns, including possible combined influences of slope, roughness, vegetation, and cultural features, offsets are provided in the GLA14 product, corresponding to alternative bin positions of the waveform, such as the beginning and end. Note that, when the GLA14 elevation product is corresponding to the

TABLE I
NUMBER OF ICESAT WAVEFORMS USED: FOREST (BROADLEAF, MIXED, AND NEEDLELEAF), URBAN, BARE LAND, AND WATER

Track	Date	Energy		Footprint			Number of corresponding pairs between ICESat and AHN data						
No.	2003	Tx (mJ)[a]	Re (fJ)[b]	Mj (m)[c]	Mi (m)[d]	Ori (deg)[e]	Broad	Mixed	Needle	Urban	Bare land	Water	Total
043	30-Sep	81	158	87	42	184	29	5	15	100	298	6	453
1233	14-Oct	77	316	99	44	11	1	19	44	216	622	7	909
1275	16-Oct	76	88	102	43	184	29	73	154	61	379	6	702
0015	23-Oct	73	54	105	44	9	4	0	0	31	212	15	262
0043	24-Oct	72	17	106	44	185	0	1	0	12	253	0	266
0295	10-Nov	66	157	100	47	186	14	3	21	110	429	3	580
						Total	77	101	234	530	2193	37	3172

[a] Transmitted energy (mJ); [b] Return energy (fJ); [c] Major (m); [d] Minor (m); [e] Orientation (degree)

waveform centroid, it is representing the mean elevation within the illuminated footprint [7]. In addition, ICESat waveforms that cause saturation of the ICESat detector result in a lower elevation [25]. A saturation elevation correction *i_satElevCorr* is applied to all GLA14 data.

To avoid large changes in surface features and land cover because of acquisition time differences, the acquisition time of ICESat data needs to be close to the acquisition time of the AHN data (1996–2003) and the CLC2000 data (1999–2001). Therefore, ICESat GLA14 and GLA01 products from campaign L2a, which were obtained in the period between September 25, 2003 and November 18, 2003, are chosen for this study. As a result, the difference in acquisition time between the data considered varies from 0 to 7 years. All data are from release 428, and the waveform data were digitized in 544 bins. In Table I, the orientation and length of the major and minor axes of the ellipses describing the footprint shape are given for each track.

These six ICESat ground tracks are chosen because of four reasons.

1) To be well spatially distributed over the study area.
2) To cover all different land cover classes.
3) ICESat measurements along these six tracks were relatively successful, compared with other L2a tracks (cloud cover).
4) For some of the tracks also considered, repeated tracks in subsequent campaigns are available (tracks 0015, 0043, and 0295), which allows repeating this analysis for later campaigns.

Moreover, waveforms from overlapping footprints from repeated tracks can be compared to assess terrain height changes and feature height changes and to identify further issues in the processing of ICESat data (cf. [33]). Starting 2007, AHN2 is being acquired over The Netherlands [34]. AHN2 has even better specifications than the first version of AHN used in this study. The release of AHN2 will offer good possibilities to assess the quality of the most recent ICESat campaigns.

After applying filtering constraints, as described later in Section III-G, a total of 3172 waveforms from six ICESat tracks were assigned to different land cover classes by using the CLC2000 land cover database (Table I). The transmitted energy falls from 81 to 66 mJ during the campaign. The average return energy of the waveform from each track varies from 17 to 316 fJ. Moreover, the nominal pointing angle is always about 0.3°. According to [35], given the reported pointing error of 0 ± 1.5 arcsec in data campaign L2a, ICESat elevation data have a theoretically vertical accuracy of 2.25 cm/1° incident angle and a horizontal accuracy of 4.5 m [35].

C. AHN

The AHN was acquired between 1996 and 2003 under leaf-off conditions and is based on airborne laser altimetry, with a point density of at least 1 point per 4×4 m^2 area. There are four levels of detail available, i.e., raw point cloud data and interpolated grid data at 5-, 25-, and 100-m resolution [34], [36]. In this study, the raw point cloud data are used. Over rural areas, the raw point cloud data are divided into nonground points (so-called vegetation points) and ground points. Over urban areas, no filtering is applied. Hence, both vegetation and buildings are present in the urban AHN data sets. All data are in ASCII format files with XYZ coordinates given in the Dutch coordinate system Rijksdriehoeksmeting and Normaal Amsterdams Peil (RDNAP) [37]. The accuracy strongly depends on the amount of vegetation and topography. For solid surfaces (e.g., roads and parking lots) and soft but flat surfaces (e.g., beaches and grass fields), the maximum systematic offset is 5 cm with a standard deviation of 15 cm. Over wooded areas, the maximum systematic offset is 10 cm with a standard deviation of 20 cm in case of at least one ground point per 36 m^2 [34].

D. CLC2000

The CLC2000 was developed by the European Environment Agency and the European Joint Research Centre. The CLC2000 database originates from the year 2000 but is actually obtained during a three-year period from 1999 to 2001, with a horizontal geolocation accuracy of 25 m based on satellite images of Landsat-7 Enhanced Thematic Mapper Plus with 25-m pixel resolution. The CLC2000 data product is obtained from Landsat data via a computer-assisted visual interpretation of the satellite images, under the requirements of a scale of 1 : 100 000, a minimum mapping unit of 25 ha, and a pixel resolution of 100 m [38]. The CLC2000 classification is hierarchical and distinguishes 44 classes at the third level, 15 classes at the second level, and five classes at the first level. Detailed information of land cover levels can be found on the metadata section on the European

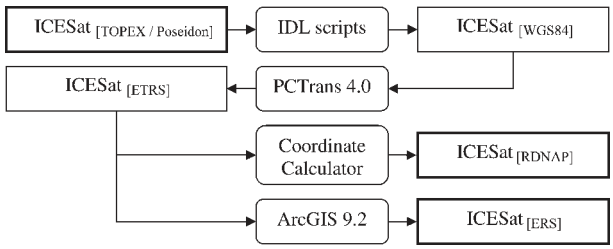

Fig. 2. Procedure of coordinate system conversion.

Environment Agency website [29]. The total thematic accuracy of the CLC2000 database was almost 95%. The database is georeferenced in the European reference system (ERS) [39].

III. Methodology

A. Datum Transformation and Coordinate Systems

A critical step in the elevation comparison is coordinate system conversion. For comparison between ICESat and AHN data with respect to land cover type from CLC2000, data sets need to be available in the same georeferenced coordinate system. AHN and CLC2000 data are available in RDNAP and ERS coordinates, respectively. Because AHN data and CLC2000 are very large data sets, ICESat data that are initially in the TOPEX/Poseidon reference frame, are chosen to be converted. ICESat data are both converted to RDNAP and ERS coordinates. The conversion scheme is shown in Fig. 2. The ICESat data in the TOPEX/Poseidon ellipsoid are first converted to the WGS84 ellipsoid by Interactive Data Language scripts provided by NSIDC [40]. This conversion produced a very small error of less than 1 cm [41]. Then, the ICESat data in WGS84 coordinates are converted to the ETRS89 reference system by the program PCTrans 4.0 [42]. The accuracy of this step is up to the centimeter level. Next, these data are transformed to the RDNAP system by the Coordinate Calculator developed in [37]. This conversion is accurate within 1 cm [43]. The total accuracy of the previous steps is still restricted to the centimeter level; therefore, this error component cannot be considered very significant to the comparison. Moreover, the ICESat GLA14 data in ETRS89 system are additionally converted to the ERS coordinates by ArcGIS 9.2 [44]. The ICESat geolocation accuracy of about 4.5 m is well below the CLC2000 resolution of 100 m. Therefore, this conversion has no significant effect either. Finally, the ICESat data are assigned to land cover type classes by comparison to the CLC2000.

B. Georeferenced Waveform

Typically, one position on the time axis of each waveform is used to compute a range between the GLAS sensor and the Earth surface, which is the so-called reference point. Together with the ICESat orbit position and orientation, elevation data, such as that available in GLA14, can be obtained [32]. To be able to use different positions in one waveform for different comparisons, this paper proposes a two-step approach: First, a waveform is registered into the RDNAP coordinate system using the reference point (the waveform centroid in most cases).

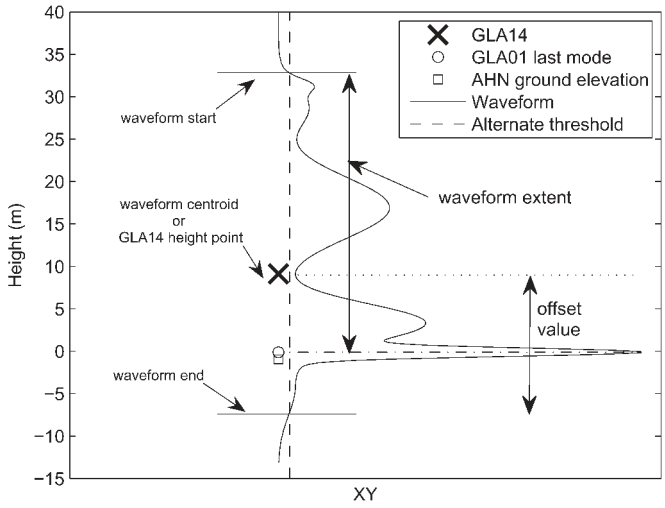

Fig. 3. (Solid line) The waveform is georeferenced by matching (horizontal dotted line) the waveform centroid to (cross) a GLA14 elevation point. The GLA01-derived elevation is (circle) the centroid of the last peak. The waveform start and waveform end are defined by threshold crossing locations.

In the second step, a suited position in the waveform is extracted. Now, the height in RDNAP of this position is simply established by considering the difference to the reference point.

In Fig. 3, the ICESat GLA14 elevation is represented by a cross; the square represents the mean AHN elevation of the ground points within the ICESat footprint. For georeferencing of the waveform (solid curve), the GLA14 reference point (here, the waveform centroid displayed by the horizontal dotted line) is matched with the GLA14 elevation point. The reference point is obtained by adding the land range offset of *i_ldRngOff* to the reference range of *i_refRng* in the GLA14 product. Which position in the waveform is used as the reference point is indicated by the elevation definition flag of *i_ElvFlg* [45].

C. Derivation of GLA01-Based Elevation Data (ICESat Last Mode)

A georeferenced waveform is decomposed into a maximum of six Gaussian components, which allows deriving waveform parameters, such as the amplitude, width, and location of each Gaussian mode. The waveform decomposition method described in detail in [46] is applied in this research. The first threshold crossing in the ICESat waveform usually corresponds to the highest intercepted surface within the footprint. The centroid of the complete waveform corresponds to the average height of the objects in the footprint, whereas the last Gaussian mode results from the lowest elevation in the footprint [2]. Over flat terrain, the lowest elevation is the ground surface if the terrain is bare. As Dutch topography is, in general, flat, the last mode is the most suitable representation of the ground elevation.

D. Derivation of Lowest Ground Surface From AHN Data (AHN Lowest Segment)

An average ICESat footprint from campaign L2a contains approximately 700 AHN data points with an average point density of 0.20 point/m^2. As stated before, there exists no AHN ground point product over urban areas. Moreover, over complex

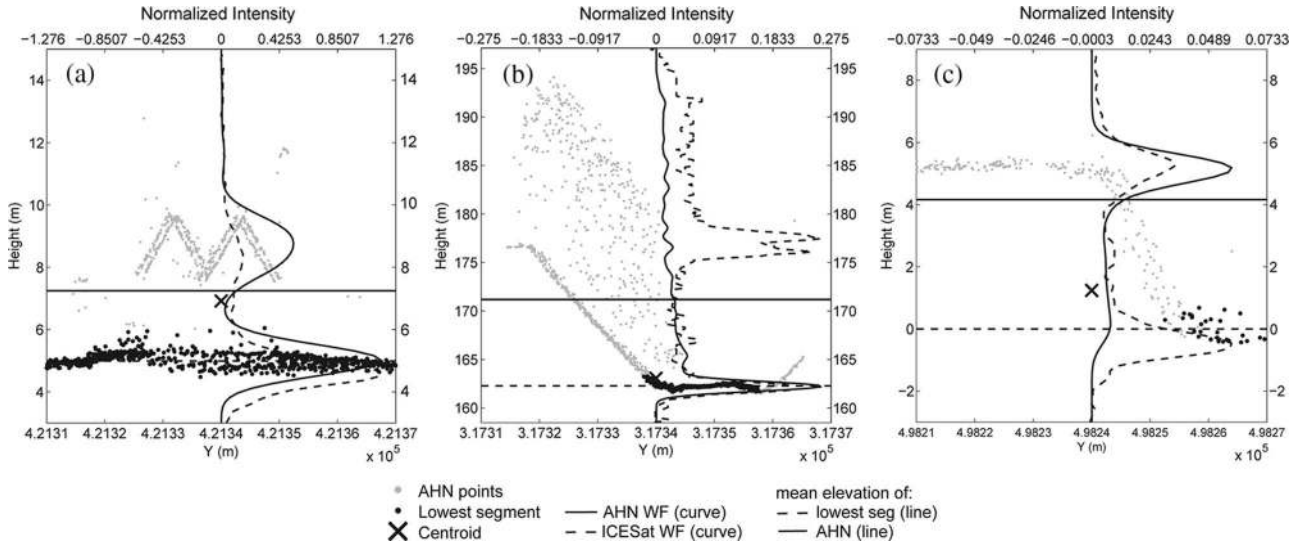

Fig. 4. (Gray dots) AHN points and (horizontal solid line) their mean height, and (black dots) the lowest segment points and (horizontal dashed line) their mean height are displayed with (solid curve) the AHN simulated waveform and (dashed curve) the ICESat waveform. (a) City with roofs and trees. (b) Canal with vegetation on the embankment. (c) Staired surface.

topography, the average height of the AHN ground points is often not representative for the height of the last mode of the ICESat waveform. Some typical examples are shown in Fig. 4. Fig. 4(a) shows an "urban" waveform. In the corresponding AHN data, different height levels are visible, e.g., from trees (left), actual ground surface (black dots), and building roofs (middle). The mean elevation of this discontinuous data set ($\sim$7.5 m) is not representative for the ICESat last mode height ($\sim$5 m). In Fig. 4(b), the ground level data (gray dots) are continuous but varying in height due to the presence of a canal in the footprint. The elevation of the horizontal bottom (black dots) is about 163 m, instead of 172 m, for the mean ground surface. Similarly, Fig. 4(c) has a series of steps in the surface elevation. The elevation of the lowest surface (black dots) is about 0 m, instead of 4 m, for the mean of the surface. Compared to the ICESat last mode, the segment containing the black points is most suitable for the comparison and, therefore, chosen as a good representative for the lowest surface.

This lowest surface is determined in two steps: First, the complete data set of AHN points (ground and nonground points) within the ICESat footprint is subdivided into many small homogeneous segments by applying a segmentation method [47]. Then, the segment containing at least ten points that has the smallest average height is selected as the lowest surface. The mean elevation of this segment is called the "AHN lowest segment." Fig. 4 shows a visualization of the AHN points (gray dots), the lowest segment points (black dots), the mean height of the AHN points (horizontal solid line), the mean height of the lowest segment (horizontal dashed line), and both the ICESat waveform (dashed curve) and the waveform simulated (solid curve) from the AHN data, as introduced in the next section.

E. Waveform Simulation From AHN Data

AHN data are used to simulate a full waveform for the purpose of feature height comparison. The full waveform is simulated in three steps: First, a power distribution corresponding to the Gaussian shape of the transmitted ICESat pulse within the footprint is applied to assign weight values to the AHN elevation points. The power distribution falls off at the footprint boundary by about $1/e^2$. Second, the histogram of AHN weighted elevation frequencies of all AHN points within a footprint area is determined. In the third step, this histogram is convolved with the emitted pulse of the corresponding ICESat waveform. As shown, for example, in [48], a returning laser altimetry waveform is the convolution of the emitted signal with the differential cross section. Next to the unknown surface reflection properties, the differential cross section depends on the height spread of the objects in the footprint, which is approximated by the height histogram of AHN height points, i.e.,

$$y = h \bullet t \tag{1}$$

where h is the histogram of heights (signal), and t is the ICESat transmitted pulse (impulse response). The convolution operator is denoted by $\bullet$, whereas y represents the resulting simulated waveform.

Fig. 5 demonstrates the waveform simulation procedure, using a bin size of 15 cm. The histogram of weighted heights h is constructed from the AHN points within the ICESat footprint [Fig. 5(a)]. Next, this histogram is convolved with the emitted pulse t, as shown in Fig. 5(b), resulting in a delayed signal displayed as a dotted curve in Fig. 5(c). The georeferenced simulated waveform is the delayed waveform shifted to the left by half the range of the transmitted pulse (24 ns $\times$ 0.15 m $= 3.6$ m), as represented by the thick black curve in Fig. 5(c). Compared to the histogram, this simulated waveform is smoother. A more advanced method of waveform simulation can be found in [49]–[51].

Two typical simulated waveforms are shown in Fig. 6. The shape of the AHN simulated waveform (solid curve) over bare land is quite similar to the corresponding ICESat waveform (dashed curve) [see Fig. 6(a)]. However, when comparing

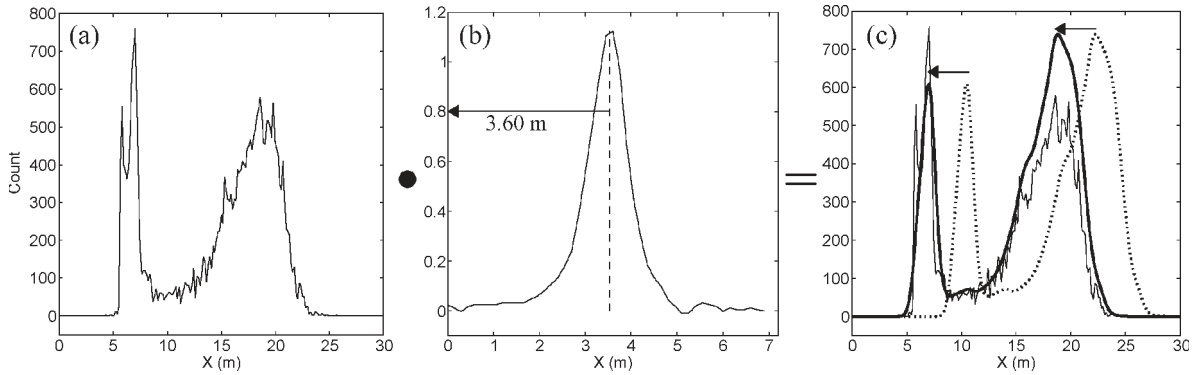

Fig. 5. Waveform simulation. (a) Histogram of height frequencies. (b) Emitted pulse as impulse response of the GLAS system. (c) Simulated waveform displayed with (thick black curve) the histogram and (dotted curve) the convolved result.

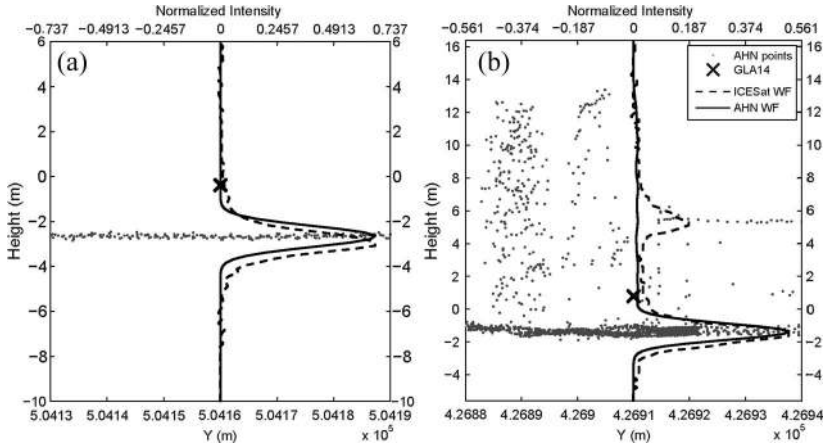

Fig. 6. (Solid curve) AHN simulated waveform and (dashed curve) ICESat waveform displayed with (gray dots) AHN points over (a) bare land and (b) forest.

ICESat and simulated AHN waveform examples over urban [Fig. 7(a)] and forest [Fig. 6(b)] areas, differences can be observed in the width and amplitude of the modes, respectively. The first mode represents the vegetation echo, and the last mode represents the ground echo. Several factors may cause a difference between the ICESat and AHN first mode.

1) Changes in the topography between two acquisition times (0–7 years).
2) The AHN data contain only airborne laser points resulting from the first and last echo data. Reflections from intermediate scatterers were not available. This may explain why the energy of the ICESat waveform does not drop to the same low level as the simulated waveform.
3) Contamination of the AHN data by multipath effects or indirect reflections.
4) The differences in the width of the last mode may also depend on the season. If most energy is reflected in the canopy, less is left for reflection from the ground.
5) Albedo effects: In Fig. 6(b), the result at a height of 5 m shows that the upper mode of the ICESat waveform is bigger than the corresponding mode of the simulated waveform.

However, over inhomogeneous areas, differences in the reflectivity of features or scatterers in the ICESat footprint may decrease or increase the amount of signal at a certain height in the ICESat waveform when compared with the AHN response, where laser points are only weighted with respect to the theoretical distribution of the energy in the corresponding emitted ICESat pulse. In Fig. 6(b), there are two different kinds of objects contributing to this first mode, i.e., the roof of a factory (horizontally aligned points at 5-m height) and trees. If the relative intensity of the AHN points would be available and could be taken into account, the roof will increase the amount of signal at the first mode.

F. Definition of Feature Heights

Precise extraction of feature heights over forest and urban areas is a challenging task. Here, it is considered how to parameterize feature height using suited waveform and point cloud parameters and how to consecutively derive these parameter values using the indicated waveform processing method. It is also shown, however, that it is very difficult to parameterize feature height in a uniform way such that feature heights can automatically be extracted, giving satisfactory results for many individual waveforms. Feature heights are both extracted from ICESat full waveforms and AHN simulated waveforms.

When using airborne laser point cloud data, such as the AHN data, over forested areas, the forest height can be defined with respect to the point cloud as the distance between the maximum and minimum elevations of the laser points. If the surface is flat or has a constant slope, the forest height can easily be extracted. In contrast, if the terrain topography contains, for example,

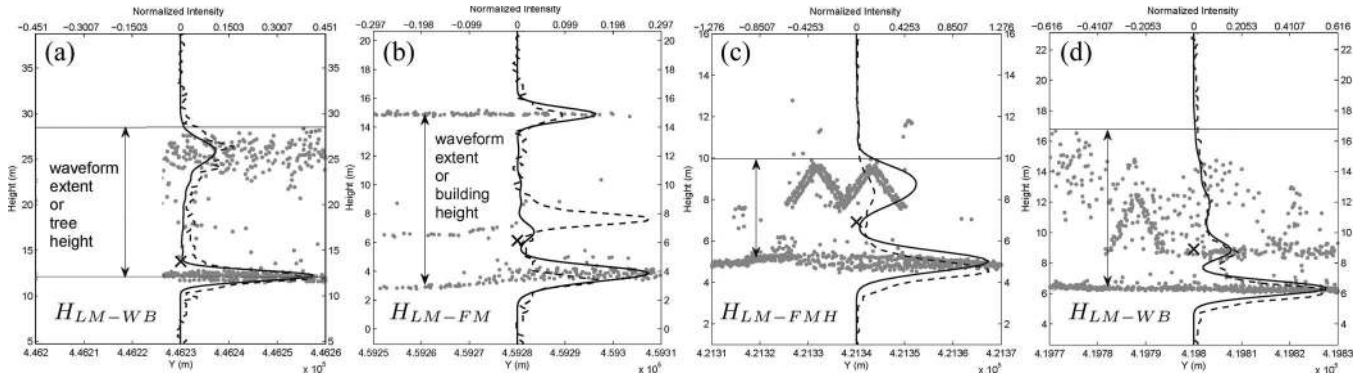

Fig. 7. Definitions of feature heights are visualized. (a) Forest height $H_{\mathrm{LM-WB}}$. (b) Building height with a flat roof $H_{\mathrm{LM-FM}}$. (c) Building height with a tilted roof $H_{\mathrm{LM-FMH}}$. (d) Building height in which the tree is higher than the building $H_{\mathrm{LM-WB}}$. Moreover, the (dashed line) ICESat waveform and (solid line) AHN simulated waveform are displayed, together with (black dots) the AHN points.

a series of steps or is subject to a varying surface slope, the definition and determination of the ground surface are critical aspects for forest height extraction [52], and more advanced methods of, for example, canopy height modeling need to be applied for precise forest height extraction [28], [53]. Moreover, over urban areas, the feature height is more complicated to define. Even when the underlying terrain height can sufficiently be determined [47], [54], the building height extraction is still in question. The distance from the terrain to the highest elevation point in the AHN point cloud is expected to represent the building highest point. However, this highest AHN elevation point could also correspond to high trees or other nonbuilding objects.

When using the ICESat full waveform, it should be taken into account that the slope and roughness of the terrain surface and variabilities in the upper parts of tree canopies are all having a widening effect on the full waveform. To enable a fair comparison to feature heights derived from the AHN point cloud, at least the slope/roughness effects need to be corrected in advance [4], [55].

Because of these different potential problems in comparing feature heights derived from the AHN point cloud to the ICESat full waveform, a simpler approach that directly compares waveform parameter values extracted from both the ICESat waveform and the AHN simulated waveform is proposed. Because the topography over The Netherlands is, in general, flat, the effect of the slope is not expected to significantly contaminate the obtained feature heights.

To be able to compare feature heights in Section IV-C, feature heights extracted from the ICESat and AHN simulated waveforms are introduced in this section. A feature height over forest is called and expected to represent forest height. Over urban areas, building heights are considered, and over bare land, low vegetation heights are considered (e.g., scrubs and bushes).

Over forest, the waveform extent, which is the vertical distance between the waveform beginning and the waveform end, as identified by threshold values, was used in [7] to estimate the maximum forest height. Due to the effects of surface slope and the variability of upper canopy parts, an SRTM-derived terrain index and the leading edge of the waveform were applied to correct the waveform extent.

To facilitate the introduction of feature heights, we define the following abbreviations for the significant waveform parameters: Waveform beginning WB is the position where the ICESat waveform first crosses the threshold value (Fig. 3). Position FHM is the location in the ICESat waveform where the waveform reaches half of the first maximum [first half maximum (FHM)] energy of the first mode [Fig. 7(c)]. Moreover, the peaks of the ICESat first and last modes are denoted as FM and LM, respectively, [Fig. 7(b)].

As discussed in the previous section, the ICESat last mode LM is most suited to represent terrain height. Therefore, forest height $H_{\mathrm{LM-WB}}$ is defined as the vertical distance between ICESat last mode LM and waveform beginning WB [Fig. 7(a)]. For bare land, low vegetation height $H_{\mathrm{LM-WB}}$ is defined in the same way.

Over urban areas, an ICESat footprint may represent not only parts of different buildings but also high trees. Three typical cases can be identified, with each consisting of footprints dominantly containing 1) a building with a flat roof (factory); 2) buildings with tilted roofs (typically Dutch residence house); and 3) a combination of high trees and buildings. To obtain a suited descriptive parameter for a building height, three potential parameters of building heights are defined. For example, in the first case, as shown in Fig. 7(b), a suited building height is the distance between the last mode LM and the first mode FM, i.e., $H_{\mathrm{LM-FM}}$. In the second case [Fig. 7(c)], the most suited building height can be the distance between the last mode LM and position FHM, i.e., $H_{\mathrm{LM-FMH}}$. In the third case, the feature height is $H_{\mathrm{LM-WB}}$ if the tree is higher than the building roof [Fig. 7(d)] or $H_{\mathrm{LM-FMH}}$ if the building is higher than the tree [Fig. 7(c)].

The feature heights of three land cover classes (forest, urban, and bare land) are summarized here.

$H_{\mathrm{LM-WB}}$ is applied for forest, urban, and bare land areas. Moreover, over urban areas, results from two additional feature height parameters $H_{\mathrm{LM-FM}}$ and $H_{\mathrm{LM-FMH}}$ are compared. The parameter that is most suited to describe the feature height over urban areas will be discussed and chosen in Section IV-C.

To enable a feature height comparison, the feature heights are also extracted from the AHN data. For this purpose, the AHN points within an ICESat footprint are simulated to a waveform,

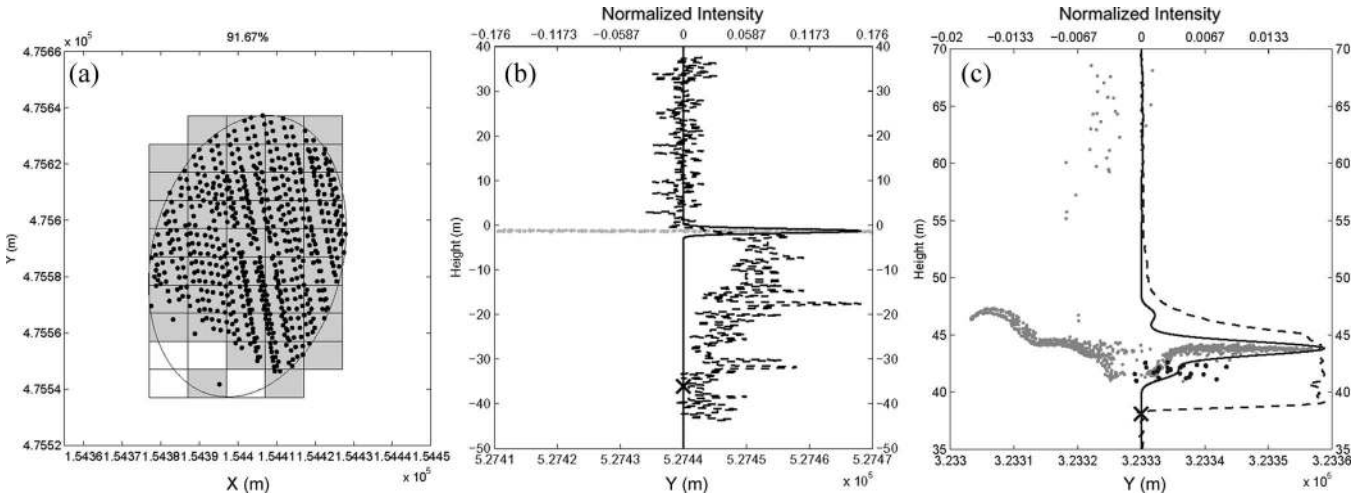

Fig. 8. (a) Coverage of the ICESat footprint by AHN points. (b) Cloud presence resulting in a height difference $\geq$ 10 m. (c) Saturated waveform with a saturation flag value of 3. The range of saturation, between 39 and 45 m, is clearly visible.

as described in Section III-E. Then, feature heights from these simulated waveforms are extracted in the same way as the ICESat waveforms. The resulting ICESat and AHN feature heights are compared in Section IV-C.

G. Filtering Constraints

To only use reliable height values for a comparison between AHN and ICESat data, constraints on both data sets are taken into account. In this research, both data sets must satisfy four conditions.

C1) All ICESat data must be considered valid, as indicated by the elevation use flag *i_ElvuseFlg*.

C2) AHN points must be well spatially distributed within the ICESat footprint. For this purpose, the footprint extent area is regularly divided into 10×10 m boxes. An ICESat footprint is removed from further comparison if 1) the number of AHN points in the ICESat footprint is less than 50 or 2) the ratio between the number of boxes containing AHN points and the total number of boxes is less than 90%. Fig. 8(a) shows a footprint where the coverage of the AHN points within the ICESat footprint is about 91%.

C3) Cloudy sky conditions may cause errors in the elevation data by effects of absorption, forward scattering, and signal delay [56]. Fig. 8(b) shows a very noisy waveform (dashed curve) obtained under cloudy conditions, resulting in a low return energy. Therefore, only those ICESat waveforms that are not effected by cloud cover are incorporated. A gain value of less than 100 counts, as indicated by the gain value of *i_gval_rcv*, is used to identify clear sky conditions [57].

C4) ICESat waveforms that saturate the ICESat detector result in a lower elevation [25]. Fig. 8(c) shows an ICESat waveform (dashed curve) and an AHN simulated waveform (solid curve) where comparison to the AHN lowest surface (black dots) suggests that saturation results, in this case, in a height jump from 42 to 40 m. Hence, ICESat waveform data should not to suffer from saturation. A GLA14 flag *i_satCorrFlg* value of 0 indicates that no saturation has occurred while receiving the waveform signal. Only waveforms with an *i_satCorrFlg* value of 0 are kept for comparison.

In the next section, two comparisons are considered.

Case 1) ICESat last mode $\leftrightarrow$ AHN lowest segment.

Case 2) ICESat feature height $\leftrightarrow$ AHN feature height.

In all comparisons, constraints C1–C4 are explicitly applied, and an AHN elevation is always subtracted from the corresponding ICESat elevation to obtain an ICESat–AHN height difference.

IV. Results and Comparison

A. Case 1: Comparison of the ICESat Last Mode and the AHN Lowest Segment

In this section, we compare the ICESat last mode elevation to the AHN lowest segment elevation, as described in Section III-D. Both elevations are considered to represent the terrain height. The ground surface is assumed to be stable between the AHN and ICESat acquisition times although the difference in acquisition ranges between 0 and 7 years. It is moreover assumed that the AHN data are accurate when compared with ICESat data. Therefore, this comparison describes the accuracy of ICESat data over terrain surface with respect to different land cover types. However, there are still outliers in the comparison, such as errors in waveform fitting [missing last mode; see Fig. 9(a)], effects of slope or rough surfaces where the last peak is higher than the mean elevation of the lowest segment [see Fig. 9(b)], and errors in segmentation [the small segment in black dots is not representative for the sloped surface; see Fig. 9(c)]. Therefore, the Median/MAD robust technique [58] is applied to discard outlier effects to arrive at realistic statistics. After applying filtering constraints C1–C4, 3172 footprints remain. The final results are given in Table II and in the histograms in Fig. 10.

The results show that it is possible to derive the terrain surface height with a bias of about 21 cm and a standard deviation of 20 cm over bare land from the ICESat altimetry

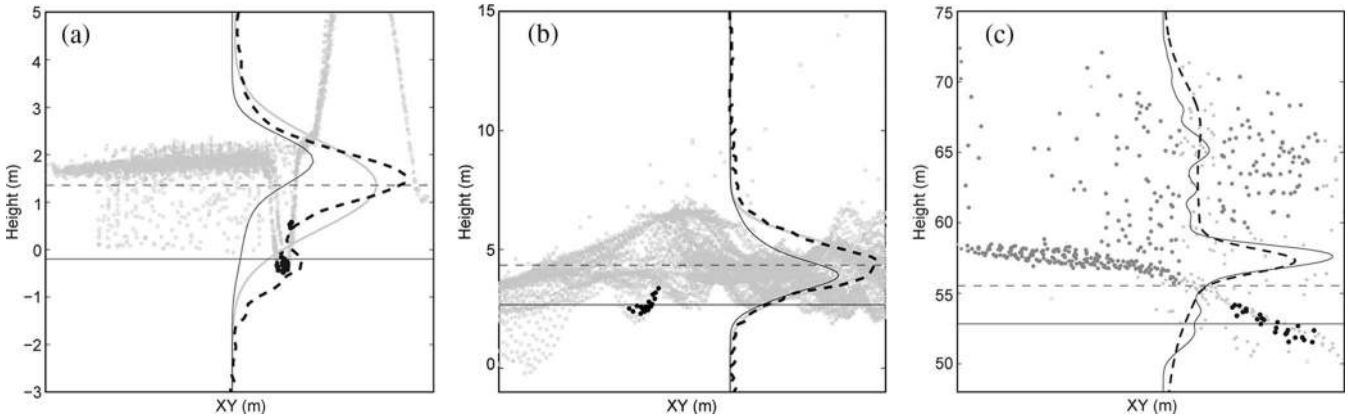

Fig. 9. Examples of outliers in the ICESat–AHN comparison. (Dashed black curve) ICESat waveform. (Solid black curve) AHN simulated waveform. (Horizontal dashed line) Mean elevation of the ICESat last mode. (Solid black line) Mean elevation of the AHN lowest segment. (a) The ICESat last mode at −0.2 m is not extracted because of fitting errors. (b) The AHN lowest segment does not give a good corresponding elevation, compared with the ICESat last mode. (c) The AHN lowest segment is not well defined for a sloped surface.

TABLE II
HEIGHT DIFFERENCE AND ITS STANDARD DEVIATION IN PARENTHESIS BETWEEN ICESAT LAST MODE AND THE AHN LOWEST SEGMENT

Track	Date	Conditions C1–C4: ICESat last mode – AHN lowest segment, (m)					
No.	2003	Broad	Mixed	Needle	Urban	Bare land	Water
043	30-Sep	−0.16 (0.92)	−0.21 (0.11)	−0.21 (0.20)	−0.51 (0.51)	−0.25 (0.20)	−0.28 (0.58)
1233	14-Oct	1.27 (0.00)	−0.34 (1.21)	−0.09 (0.23)	−0.22 (0.20)	−0.22 (0.16)	−0.26 (0.03)
1275	16-Oct	−0.12 (0.15)	0.15 (0.67)	0.01 (0.34)	−0.18 (0.32)	−0.16 (0.22)	−0.17 (0.29)
0015	23-Oct	0.31 (0.63)	N/A	N/A	0.21 (0.53)	−0.09 (0.35)	0.21 (0.20)
0043	24-Oct	N/A	−0.24 (0.00)	N/A	0.04 (0.32)	−0.18 (0.20)	N/A
0295	10-Nov	−0.30 (0.82)	−0.24 (0.51)	−0.19 (0.30)	−0.28 (0.24)	−0.30 (0.21)	−0.59 (0.58)
	Total	−0.14 (0.59)	−0.11 (0.69)	−0.07 (0.30)	−0.24 (0.28)	−0.21 (0.20)	−0.08 (0.34)
Number of pairs		77	101	234	530	2193	37

data. Over forest, the height difference is, on average, 14 cm for broadleaf, 11 cm for mixed, and 7 cm for needleleaf. The standard deviation value is, however, large over broadleaf (0.59 m) and over mixed (0.69 m), and smaller over needleleaf (0.30 m). Moreover, in the urban case, the difference in terrain height is 0.24 m with a small standard deviation of 0.28 m.

In the case of water, a small case study shown in Fig. 11 gives us several reasons to mistrust comparisons over footprints classified by CLC2000 as water: varying water levels, strongly varying numbers of AHN points over water due to absorption, appearance of structures such as boats in the water, and footprints on the border between water and land. Therefore, we conclude that comparisons for footprints marked as water are not reliable. Some waveform locations over a water body are displayed superimposed on Google Earth imagery (bottom), together with a visualization of the corresponding ICESat waveforms and AHN data (top). The green dots represent the AHN points within the ICESat footprint, and the gray dots are outside the footprint. The footprint size is indicated by the length of the horizontal black line. We make three observations.

1) Occurrence of artificial objects: In Fig. 11(a) and (b), AHN data indicate the occurrence of an artificial object (e.g., a long boat or a construction work) with a length of about 175 m (ICESat footprint spacing) over the water surface, whereas the corresponding ICESat waveform has a single peak at an elevation of −5.7 m. This object causes a height difference of 4.7 m in case of Fig. 11(a) and 0.86 m in Fig. 11(b).
2) Fig. 11(d) shows an ICESat footprint location that is classified as water. Still, this footprint contains some AHN points that originate from the land surface. As there are no AHN points over the water part of the footprint, a difference of 1.31 m occurs between the ICESat and AHN centroid elevations.
3) On the other hand, Fig. 11(c) shows a footprint that only covers water, but, still, AHN points are available, resulting in a height difference between the AHN and the ICESat centroid of 0.29 m. This difference is probably caused by a change in water level between the AHN and ICESat acquisition time (0–7 years), also comparing the consistent AHN and ICESat elevations in the neighboring footprints.

B. ICESat Incident Angle Effect

Further insight into the observed differences in ICESat- versus AHN-derived terrain height is gained by analyzing the influence of ICESat incidence angle and pointing error. According to [59], the maximum elevation error of the ICESat product

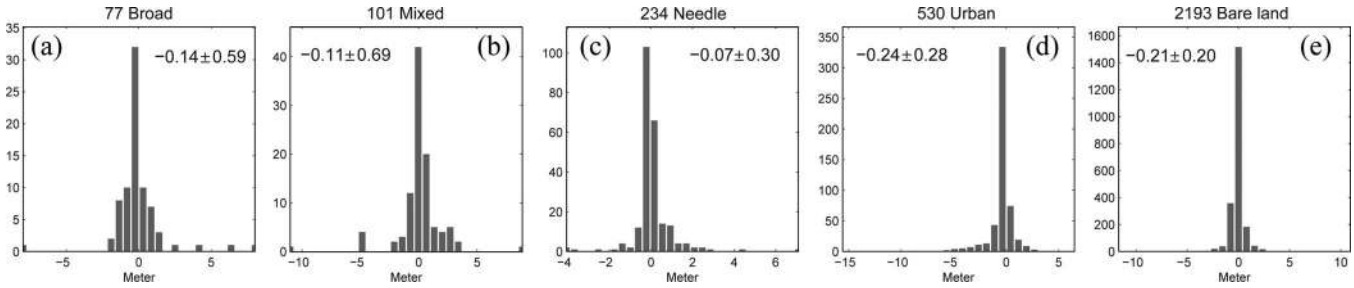

Fig. 10. Histograms of height differences obtained after applying conditions C1–C4 over (a) broadleaf, (b) mixed, (c) needleleaf, (d) urban, and (e) bare land. Median and standard deviation values have been estimated by the Median/MAD robust statistics [58].

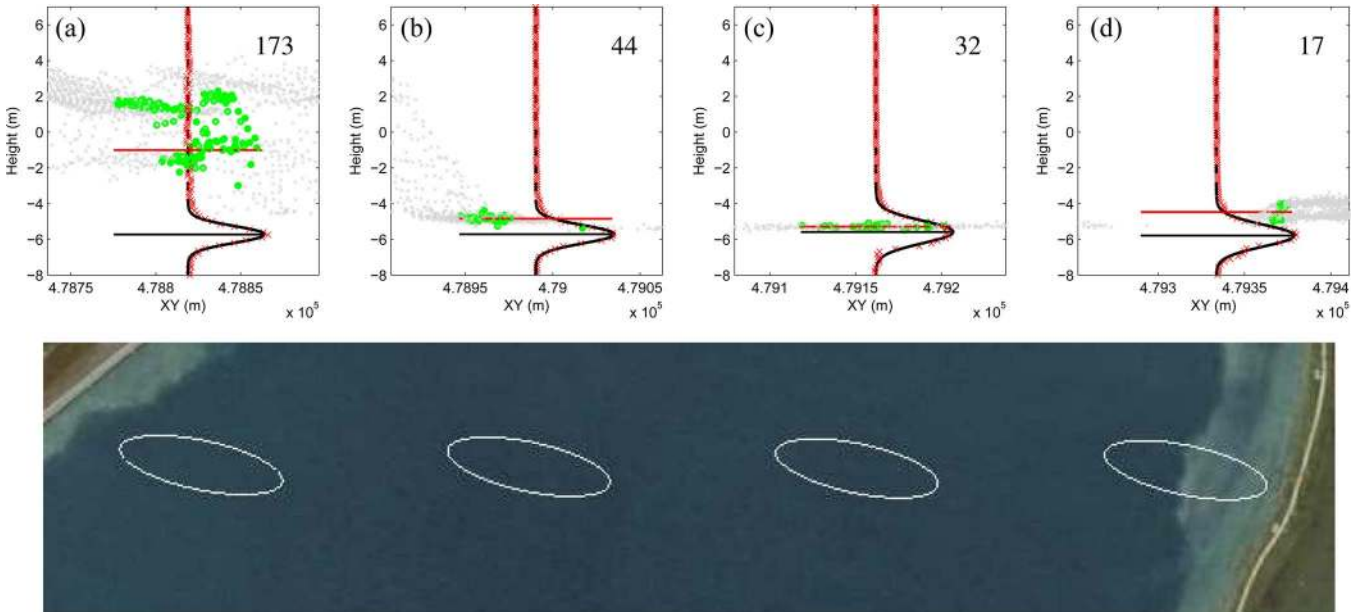

Fig. 11. (Top) Water waveforms with (top right) the number of AHN points within (bottom) the ICESat footprints displayed, together with the Google Earth image. (Horizontal black line) Last mode height. (Horizontal red line) Mean height of AHN ground points. (Green dots) AHN points located inside the ICESat footprint. (Gray dots) AHN points outside the ICESat footprint.

is equal to about 7.5 cm/1° incident angle with a laser pointing error of 1.5 arcsec. To limit the impact of incident angle on elevation errors to an effect of maximally a few centimeters, footprints were removed if the ICESat incident angle is larger than 1°. By using the AHN data, the ICESat incident angle is obtained from a combination of the ICESat laser pointing angle and the AHN surface slope. The AHN surface slope is obtained by fitting a plane to the AHN lowest segment data within the footprint.

In comparison to the previous results, the results show that the observed differences in terrain height are strongly changed in forested areas and slightly improved in bare land and urban areas. Over forested areas, the average difference slightly increases, i.e., by 13 cm over mixed forest and 5 cm over both needleleaf and broadleaf forests. The standard deviation is significantly reduced from a maximum of 69 cm (over mixed) to a maximum of 25 cm (over broadleaf). Moreover, over urban and bare land areas, only the standard deviation is reduced by 1–5 cm. The price to pay for the improvement in the statistics is that 873 pairs were removed from a total of 3172 pairs. Although this analysis was performed over relatively flat terrain, it demonstrates that the ICESat incidence angle has an impact on the accuracy of the terrain height.

C. Case 2: Comparison Between the ICESat- and AHN-Derived Feature Heights

In this section, after applying filtering constraints C1–C4, 3172 feature heights derived from ICESat waveforms and AHN simulated waveforms, as defined in Section III-F, are compared. Histograms of forest, building, and low vegetation heights using parameter $H_{\mathrm{LM-WB}}$ are shown in Fig. 12(a)–(c), respectively. On average, the feature height is about 17–20 m over forest, 8–9 m over buildings, and almost 3 m over low vegetation.

Table III shows height differences with respect to forest, buildings, and low vegetation in terms of feature height parameter $H_{\mathrm{LM-WB}}$. Moreover, over urban areas, two other feature height parameters $H_{\mathrm{LM-FM}}$ and $H_{\mathrm{LM-FMH}}$ were also determined. According to the feature height $H_{\mathrm{LM-WB}}$, the height difference between the ICESat data and AHN data is equal to 1.89 m over forest, 1.48 m over buildings, and 29 cm over low vegetation. The standard deviation is larger over buildings

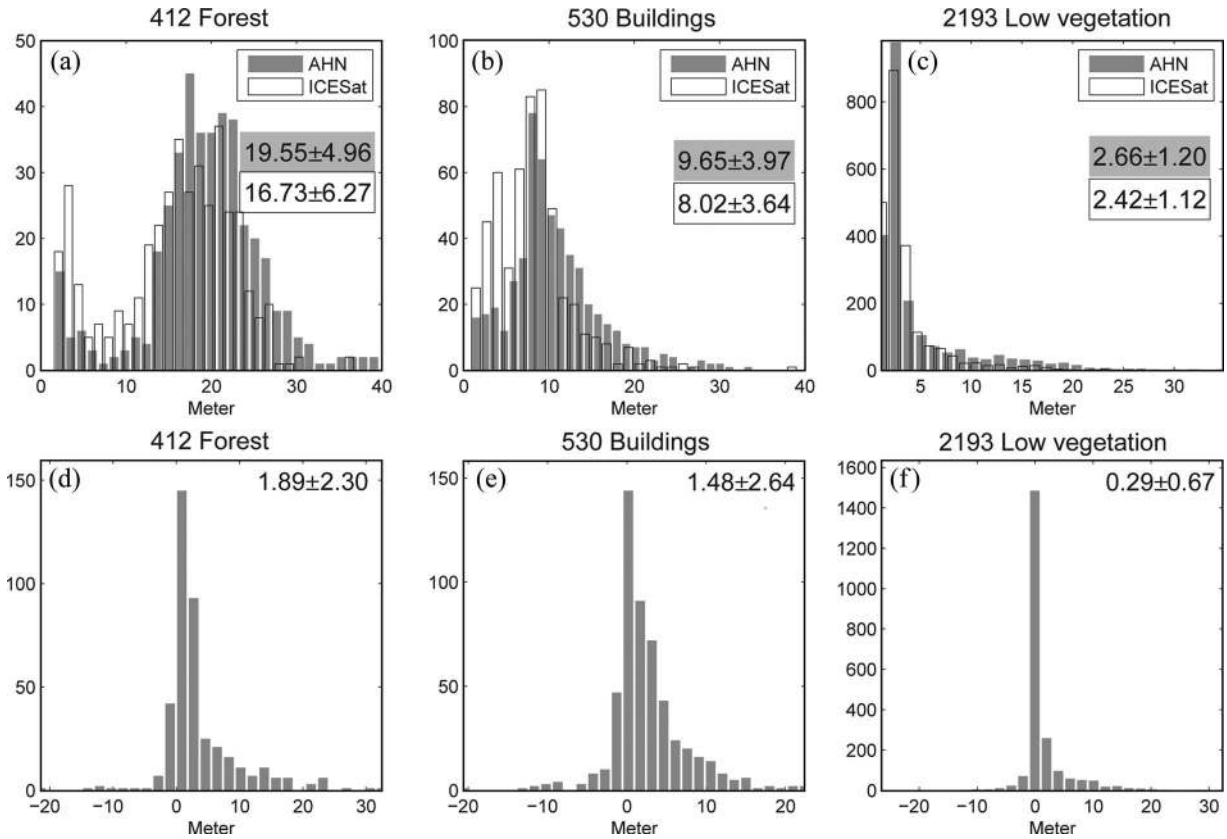

Fig. 12. Histograms of feature heights extracted from AHN and ICESat data for (a) forest, (b) buildings, and (c) low vegetation. (Gray) Histograms of the AHN feature heights. The ICESat histograms are bounded by a solid black line. For both AHN and ICESat, the mean value and standard deviation are given in the corresponding text boxes. Moreover, the histograms of $H_{\mathrm{LM-WB}}$ feature height differences between AHN and ICESat data are shown in (d)–(f) for different terrain classes. In each plot, the Median/MAD value is indicated.

TABLE III
FEATURE HEIGHT DIFFERENCE AND ITS STANDARD DEVIATION IN PARENTHESIS BETWEEN ICESAT AND AHN

By	Forest	Urban	Low vegetation
H_{LM-WB}	1.89 (2.30)	1.48 (2.64)	0.29 (0.67)
H_{LM-FM}	N/A	0.40 (3.75)	N/A
H_{LM-FMH}	N/A	1.06 (3.19)	N/A

(2.64 m) and forest (2.30 m), and small over low vegetation (67 cm). Compared to the mean feature heights, as shown in Fig. 12(a)–(c), respectively, the height difference over forest and bare land is 10%. However, over urban areas, a height difference of 1.48 m is notably larger, compared with a feature height on the order of 8–9 m.

Using the feature height parameters $H_{\mathrm{LM-FM}}$ and $H_{\mathrm{LM-FMH}}$ over urban terrain leads to a reduction of the mean height difference to 40 cm for $H_{\mathrm{LM-FM}}$ and 1.06 m for $H_{\mathrm{LM-FMH}}$. However, the standard deviations are increasing to 3.75 m for $H_{\mathrm{LM-FM}}$ and 3.19 m for $H_{\mathrm{LM-FMH}}$.

We conclude that none of the three feature height parameters defined for buildings give very satisfactory results. Several reasons explain this negative outcome. A first reason is that, for different scenarios (like first intercept is flat roof, tilted roof, or urban tree), different feature height parameterizations are more suited. Therefore, applying one parameterization for all possible scenarios will definitely result in suboptimal outcomes. Unfortunately, it seems, in practice, impossible to classify an urban waveform as corresponding to a certain scenario. Still, this reason does not explain differences in urban feature height, as derived from either ICESat or AHN simulated waveforms.

The large standard deviation of the building height differences can be explained by the following circumstances: 1) Small geolocation errors. With a small shift in footprint location, parts of other buildings may appear in the footprint, causing different height levels. 2) Feature changes that occurred between ICESat and AHN acquisition times (0–7 years) are particularly likely in urban areas, considering, e.g., new built-up houses, removed/renovated old houses, and artificially added or removed trees (see Fig. 13). 3) Due to the absence of intensity values in the AHN data set, the AHN simulated waveform is not always comparable to the ICESat waveform [see Fig. 6(b)], particularly when the ICESat footprint is partly covering a building roof with a strong reflection. The energy return from such roof is recorded as the dominant peak in the ICESat waveform. However, the few reflecting points present in the AHN data are not enough to obtain such a dominant peak in the simulated waveform. The missing peak causes a large height difference in the feature height comparison.

To improve the feature height comparison, an additional condition could be implemented. Since the AHN data were acquired during 1996–2003, spanning a larger time window, compared with the ICESat data acquired approximately in a one-month period, it is likely that, in some cases, actual feature

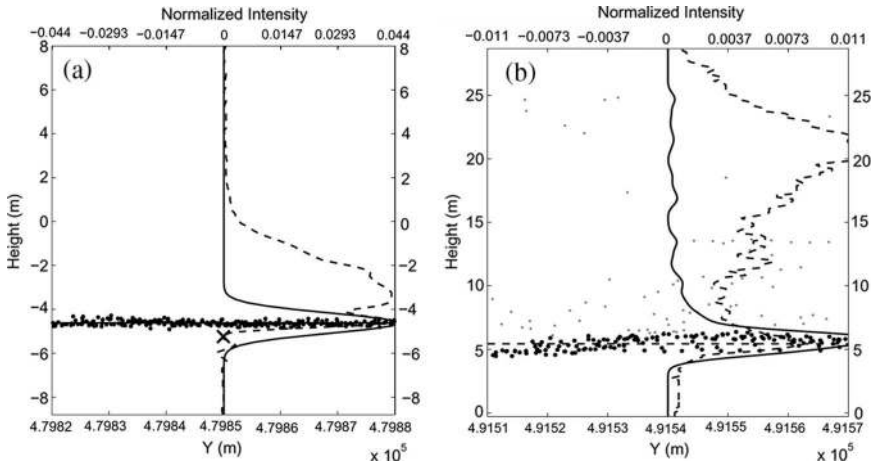

Fig. 13. Big changes on the Earth surface. (a) (Solid line) The AHN waveform is simulated from (black dots) the AHN points that do not contain any data points from above the terrain surface. However, (dashed line) the ICESat waveform properly includes other objects, e.g., new houses. (b) Similarly, very few vegetation points in the AHN data correspond to a weak peak in the AHN simulated waveform; however, there seems to occur, e.g., new trees in the ICESat waveform.

height changes occurred between the AHN and ICESat acquisition. This could lead to anomalous feature height differences. The AHN and ICESat terrain heights, as derived for the terrain height comparison, can be applied to match ICESat and AHN simulated waveforms corresponding to (actual) terrain height. Considerable differences between the two waveform shapes can now easily be identified by applying a correlation coefficient threshold.

In general, one can conclude that obtaining feature heights from ICESat waveforms makes sense for either well-controlled footprint locations, where the objects represented by the ICESat waveform are known to the operator or, on the other hand, for larger populations of waveforms, representing homogeneous features, that are likely to exhibit a similar change through time, as can be expected in agricultural or forest applications. Over urban regions, where the footprint contents is expected to change from footprint to footprint, analyzing feature height for groups of waveforms together seems doubtful.

V. Conclusion

In this paper, we have compared ICESat-derived elevations to high-resolution airborne laser altimetry data over complex terrain. Airborne data have been obtained from the Dutch national airborne laser altimetry product AHN. Two comparisons have been performed: Terrain height was assessed by comparing the ICESat last mode against the AHN mean lowest segment, and ICESat feature height was evaluated against the AHN feature height.

For the terrain height, the difference between the elevation of ICESat's last mode and the mean elevation of the AHN lowest segment is, on average, -21 cm over bare land and -24 cm over urban areas, and ranges from -14 to -7 cm over forested areas. The standard deviation of the differences ranges between 20 cm for bare land and 69 cm for forested areas. This comparison has been performed on a population of several thousands of waveforms. These results show that ICESat and likely follow-up missions have good potential for measuring terrain height, even over complex forested and urban terrain with an accuracy at the decimeter range. In fact, the resulting accuracies start to approach a higher accuracy level as could be expected from airborne laser surveys.

For the feature height case, the difference between ICESat- and airborne-derived feature height is acceptable over forested and bare land areas. However, the result over buildings is not satisfactory. The main reason is that ICESat-derived feature height parameters are sensitive changes in feature height that occur at spatial distances smaller than the size of the ICESat footprints. For the homogeneous land cover type, ICESat waveform analysis is a suited method for parameterizing feature heights. For the urban case, an additionally accurate DEM data may still enable the monitoring of feature height changes.

The study of the two described comparisons demonstrates that not only can good results be obtained, on average, for large populations of waveforms together but terrain and feature height extraction of ICESat data at the single shot level is also feasible and accurate to the levels shown here. If the spatial coverage of future satellite laser altimetry missions could be improved by applying different acquisition patterns (e.g., different orbit configuration and multiple view lasers), such missions could be applied for obtaining large-scale elevation and forestry/biomass products of unprecedented accuracies.

Analysis of single waveforms is important to obtain insight on differences that still occur between ICESat waveforms and, in our case, simulated waveforms, as constructed from corresponding AHN points. The main reasons for the remaining differences in elevation in our comparison are actual changes within the footprint, which are explainable by temporal/seasonal acquisition differences, geolocation errors, inhomogeneous scattering distribution within the footprint, and atmospheric disturbances.

Note that the signed terrain elevation difference between ICESat and AHN terrain height is negative. This means that ICESat slightly underestimates terrain height. The ICESat elevation accuracy depends on saturation, atmospheric forward scattering, surface roughness, pointing errors, and field-of-view shadowing. The first two error sources were excluded in the

comparison based on quality flags provided in the GLAS product. The third and fourth error sources have been discussed in this paper. However, the last one, i.e., field-of-view shadowing, which is significant in campaign L2a data, is not analyzed yet. This factor causes distortion of the laser power distribution within the footprint, resulting in clipped/skewed waveform shapes. As a consequence, ICESat elevations can be too low by several centimeters, with a bias magnitude correlated with the footprint size and laser energy level [59]. This error source could be the remaining problem for underestimated terrain heights and, therefore, needs to be investigated and quantified in further studies. Finally, almost time-coincident data from airborne AHN2 and recent ICESat campaigns is becoming available. Repeating this analysis on these new data sets will enable obtaining better insight into error sources in ICESat height underestimation and terrain/feature height differences between ICESat and AHN data.

ACKNOWLEDGMENT

The authors would like to thank the National Snow and Ice Data Center; G. Hazeu from Wageningen University, Wageningen, The Netherlands; and the European Environment Agency for their guidelines and data distribution.

REFERENCES

[1] H. J. Zwally, B. Schutz, W. Abdalati, J. Abshire, C. Bentley, A. Brenner, J. Bufton, J. Dezio, D. Hancock, D. Harding, T. Herring, B. Minster, K. Quinn, S. Palm, J. Spinhirne, and R. Thomas, "ICESats laser measurements of polar ice, atmosphere, ocean, and land," *J. Geod.*, vol. 34, no. 3/4, pp. 405–445, Oct./Nov. 2002.

[2] A. C. Brenner, H. J. Zwally, C. R. Bentley, B. M. Csatho, D. J. Harding, M. A. Hofton, J. B. Minster, L. A. Roberts, J. L. Saba, R. H. Thomas, and D. Yi, "Geoscience laser altimeter system algorithm theoretical basis document: Derivation of range and range distributions from laser pulse waveform analysis," *Algorithm Theoretical Basis Documents (ATBD)*, 2003. [Online]. Available: http://www.csr.utexas.edu/glas/atbd.html

[3] "Frequently asked question," *ICESat/GLAS Data at NSIDC*, 2005. [Online]. Available. http://nsidc.org/data/icesat/faq.html

[4] M. Lefsky, D. Harding, M. Keller, W. Cohen, C. Carabajal, F. Espirito-Santo, M. Hunter, and R. Oliveira, "Estimates of forest canopy height and above ground biomass using ICESat," *Geophys. Res. Lett.*, vol. 32, no. 22, pp. L22 S02-1–L22 S02-4, Nov. 2005. DOI:10.1029/2005GL023971.

[5] M. A. Lefsky, W. B. Cohen, D. J. Harding, G. G. Parker, S. A. Acker, and S. T. Gower, "Lidar remote sensing of above-ground biomass in three biomes," *Glob. Ecol. Biogeogr.*, vol. 11, no. 5, pp. 393–399, Oct. 2002.

[6] J. Boudreau, R. F. Nelson, H. A. Margolis, A. Beaudoin, L. Guindon, and D. S. Kimes, "Regional above ground forest biomass using airborne and spaceborne lidar in Québec," *Remote Sens. Environ.*, vol. 112, no. 10, pp. 3876–3890, Oct. 2008.

[7] D. J. Harding and C. C. Carabajal, "ICESat waveform measurements of within-footprint topographic relief and vegetation vertical structure," *Geophys. Res. Lett.*, vol. 32, no. 21, pp. L21 810.1–L21 810.4, Oct. 2005. DOI:10.1029/2005GL023471.

[8] G. Sun, K. Ranson, D. Kimes, J. Blair, and K. Kovacs, "Forest vertical structure from GLAS: An evaluation using LVIS and SRTM data," *Remote Sens. Environ.*, vol. 112, no. 1, pp. 107–117, Jan. 2008.

[9] J. A. B. Rosette, P. R. J. North, and J. C. Suárez, "Vegetation height estimates for a mixed temperate forest using satellite laser altimetry," *Int. J. Remote Sens.*, vol. 29, no. 5, pp. 1475–1493, Mar. 2008.

[10] K. Ranson, G. Sun, K. Kovacs, and V. Kharuk, "Landcover attributes from ICESat GLAS data in Central Siberia," in *Proc. IEEE IGARSS*, Anchorage, AK, Sep. 20–24, 2004, vol. 2, pp. 753–756.

[11] V. H. Duong, R. Lindenbergh, N. Pfeifer, and G. Vosselman, "Single and two epoch analysis of ICESat full waveform data over forested areas," *Int. J. Remote Sens.*, vol. 29, no. 5, pp. 1453–1473, Mar. 2008.

[12] C. A. Shuman, H. J. Zwally, B. E. Schutz, A. C. Brenner, J. P. DiMarzio, V. P. Suchdeo, and H. A. Fricker, "ICESat Antarctic elevation data: Preliminary precision and accuracy assessment," *Geophys. Res. Lett.*, vol. 33, no. 7, p. L07 501, Apr. 2006. DOI:10.1029/2005GL025227.

[13] T. Yamanokuchi, K. Doi, and K. Shibuya, "Combined use of InSAR and ICESat/GLAS data for high accuracy DEM generation on Antarctica," in *Proc. IEEE IGARSS*, 2007, pp. 1229–1231.

[14] J. Wahr, D. Wingham, and C. Bentley, "A method of combining ICESat and GRACE satellite data to constrain Antarctic mass balance," *J. Geophys. Res.*, vol. 105, no. B7, pp. 16 279–16 294, 2000.

[15] D. C. Slobbe, R. C. Lindenbergh, and P. Ditmar, "Estimation of volume change rates of Greenland's ice sheet from ICESat data using overlapping footprints," *Remote Sens. Environ.*, vol. 112, no. 12, pp. 4204–4213, Dec. 2008.

[16] R. Bindschadler, H. Choi, C. Shuman, and T. Markus, "Detecting and measuring new snow accumulation on ice sheets by satellite remote sensing," *Remote Sens. Environ.*, vol. 98, no. 4, pp. 388–402, Oct. 2005.

[17] H. J. Zwally, D. Yi, R. Kwok, and Y. Zhao, "ICESat measurements of sea ice freeboard and estimates of sea ice thickness in the weddell sea," *J. Geophys. Res.*, vol. 113, no. C2, p. C02 S15, Feb. 2008. DOI:10.1029/2007JC004284.

[18] J. Bamber and J. L. Gomez-Dans, "The accuracy of digital elevation models of the Antarctic continent," *Earth Planet. Sci. Lett.*, vol. 237, no. 3/4, pp. 516–523, Sep. 2005.

[19] C. C. Carabajal and D. J. Harding, "ICESat validation of SRTM C-band digital elevation models," *Geophys. Res. Lett.*, vol. 32, no. 22, pp. L22 S01.1–L22 S01.5, Nov. 2005.

[20] C. C. Carabajal and D. J. Harding, "SRTM C-band and ICESat laser altimetry elevation comparisons as a function of tree cover and relief," *Photogramm. Eng. Remote Sens.*, vol. 72, no. 3, pp. 287–298, Mar. 2006.

[21] K. J. Bhang, F. W. Schwartz, and A. Braun, "Verification of the vertical error in C-band SRTM DEM using ICESat and Landsat-7, Otter Tail County, MN," *IEEE Trans. Geosci. Remote Sens.*, vol. 46, no. 1, pp. 36–44, Jan. 2007.

[22] N. T. Kurtz, T. Markus, D. J. Cavalieri, W. Krabill, J. G. Sonntag, and J. Miller, "Comparison of ICESat data with airborne laser altimeter measurements over Arctic sea ice," *IEEE Trans. Geosci. Remote Sens.*, vol. 46, no. 7, pp. 1913–1924, Jul. 2008.

[23] C. F. Martin, R. H. Thomas, W. B. Krabill, and S. S. Manizade, "ICESat range and mounting bias estimation over precisely-surveyed terrain," *Geophys. Res. Lett.*, vol. 32, no. 21, pp. L21 S07.1–L21 S07.4, Oct. 2005. DOI:10.1029/2005GL023800.

[24] L. A. Magruder, C. E. Webb, T. J. Urban, E. C. Silverberg, and B. E. Schutz, "ICESat altimetry data product verification at white sands space harbor," *IEEE Trans. Geosci. Remote Sens.*, vol. 45, no. 1, pp. 147–155, Jan. 2007.

[25] H. A. Fricker, A. Borsa, B. Minster, C. Carabajal, K. Quinn, and B. Bills, "Assessment of ICESat performance at the Salar de Uyuni, Bolivia," *Geophys. Res. Lett.*, vol. 32, no. 21, p. L21 S06, Sep. 2005. DOI:10.1029/2005GL023423.

[26] D. Atwood, R. Guritz, R. Muskett, C. Lingle, J. Sauber, and J. Freymueller, "DEM control in Arctic Alaska with ICESat laser altimetry," *IEEE Trans. Geosci. Remote Sens.*, vol. 45, no. 11, pp. 3710–3720, Nov. 2007.

[27] A. Braun and G. Fotopoulos, "Assessment of SRTM, ICESat, and survey control monument elevations in Canada," *Photogramm. Eng. Remote Sens.*, vol. 73, no. 12, pp. 1333–1342, 2007.

[28] D. J. Harding, M. A. Lefsky, G. G. Parker, and J. B. Blair, "Laser altimeter canopy height profiles: Methods and validation for closed-canopy, broadleaf forests," *Remote Sens. Environ.*, vol. 76, no. 3, pp. 283–297, Jun. 2001.

[29] European Environment Agency, *CORINE Land Cover 2000*, 2006. [Online]. Available: http://dataservice.eea.eu.int/dataservice/metadetails.asp?id=822

[30] H. J. Rim and B. E. Schutz, "Precision orbit determination (POD)," *Algorithm Theoretical Basis Documents (ATBD)*, 2002. [Online]. Available: http://www.csr.utexas.edu/glas/pdf/atbd_pod_10_02.pdf

[31] S. Bae and B. E. Schutz, "Precision attitude determination (PAD)," *Algorithm Theoretical Basis Documents (ATBD)*, 2002. [Online]. Available: http://www.csr.utexas.edu/glas/pdf/atbd_pad_10_02.pdf

[32] B. E. Schutz, "Laser footprint location (geolocation) and surface profiles," Center Space Res., Univ. Texas, Austin, Austin, TX, 2002. Tech. Rep.

[33] H. Duong, R. Lindenbergh, N. Pfeifer, and G. Vosselman, "Error analysis of icesat waveform processing by investigating overlapping pairs over Europe," in *Proc. IEEE IGARSS*, Barcelona, Spain, Jul. 23–27, 2007, pp. 4753–4756.

[34] AHN, *Actual Height Model of The Netherlands*, 2008. [Online]. Available: http://www.ahn.nl/english.php
[35] T. J. Urban, B. E. Schutz, and A. L. Neuenschwander, "A survey of ICESat coastal altimetry applications: Continental coast, open ccean island, and inland river," *Terr., Atmos. Ocean. Sci.*, vol. 19, pp. 1–19, 2008.
[36] R. Heerd, E. Kuijlaars, M. Teeuw, and R. 't Zand, "Produktspecificatie AHN," *Rijkswaterstaat, Adviesdienst Geo-informatie en ICT*, 2000.
[37] RDNAP, "Rijksdriehoeksmeting and normaal amsterdams peil," *Dutch Geometric Infrastructure*, 2007. [Online]. Available: http://www.rdnap.nl/
[38] V. Perdigão and A. Annovi, "Technical and methodological guide for updating corine land cover database," Joint Res. Centre, Eur. Environ. Agency, Copenhagen, Denmark, 1997. [Online]. Available: http://www.ec-gis.org/document.cfm?id=197&db=document
[39] G. Hazeu, "CLC2000 land cover database of The Netherlands: Monitoring land cover changes between 1986 and 2000," Green World Res., Wageningen, The Netherlands, 2003. Alterra, Alterra-rapport 775/CGI-rapport 03-006, Tech. Rep.
[40] NSIDC, *Tools for Working With ICESat/GLAS Data*, 2006. [Online]. Available: http://nsidc.org/data/icesat/tools.html
[41] J. Meeus, *Astronomical Algorithms*. Richmond, VA: Willmann-Bell, 1991.
[42] RNlN, "PCTrans 4.2.3," *Hydrographic Service of the Royal Netherlands Navy*, 2008. [Online]. Available: http://www.hydro.nl/pgS/en/pctrans_en.htm
[43] Hoog/NAP, *Nlgeo2004: Geoid Model Over The Netherlands*, 2009. [Online]. Available: http://www.rdnap.nl/algemeen/hoogte/geoide.html
[44] EEA, *EEA Reference Grids*, 2008. [Online]. Available: http://dataservice.eea.europa.eu/dataservice/metadetails.asp?id=760
[45] NSIDC, *GLAS Altimetry Data Dictionary*, 2008. [Online]. Available: http://nsidc.org/data/docs/daac/glas_altimetry/data_dictionary_rel28.html
[46] H. Duong, N. Pfeifer, and R. Lindenbergh, "Analysis of repeated ICESat full waveform data: Methodology and leaf-on/leaf-off comparison," in *Proc. Workshop 3D Remote Sens. Forestry*, 2006, pp. 239–248.
[47] T. Rabbani, F. A. van den Heuvel, and G. Vosselman, "Segmentation of point clouds using smoothness constraint," in *Int. Arch. Photogramm. Remote Sens. Spat. Inf. Sci.*, Dresden, Germany, Sep. 25–27, 2006, vol. XXXVI, pt. 5, pp. 248–253.
[48] W. Wagner, A. Ullrich, V. Ducic, T. Melzer, and N. Studnicka, "Gaussian decomposition and calibration of a novel small-footprint full-waveform digitizing airborne laser scanner," *ISPRS J. Photogramm. Remote Sens.*, vol. 60, pp. 100–112, 2006.
[49] J. B. Blair and M. A. Hofton, "Modeling laser altimeter return waveforms over complex vegetation using high-resolution elevation data," *Geophys. Res. Lett.*, vol. 26, no. 16, pp. 2509–2512, Aug. 1999.
[50] S. Filin and B. Csathó, "An efficient algorithm for the synthesis of laser altimeter waveforms," BPRC, Columbus, OH, 2002, Tech. Rep. [Online]. Available: http://bprc.osu.edu/glid/Documents/WF_simulator/Waveform_simulator.pdf
[51] J. M. Abshire, J. F. McGarray, L. K. Pacini, J. B. Blair, and G. C. Elman, "Laser altimetry simulator. Version 3.0: User's guide," *NASA Technical Memorandum 104588*, 1994. p. 66. [Online]. Available: http://ntrs.nasa.gov/archive/nasa/casi.ntrs.nasa.gov/19940021649_199402 1649.pdf
[52] M. A. Lefsky, W. B. Cohen, G. G. Parker, and D. J. Harding, "Lidar remote sensing for ecosystem studies," *BioScience*, vol. 52, no. 1, pp. 19–30, 2002.
[53] M. Hollaus and W. Wagner, "Operational use of airborne laser scanning for forestry applications in complex mountainous terrain," in *Proc. 9th Int. Symp. High Mountain Remote Sens. Cartography*, 2007, pp. 19–26.
[54] K. Kraus and N. Pfeifer, "Determination of terrain models in wooded areas with airborne laser scanning data," *ISPRS J. Photogramm. Remote Sens.*, vol. 53, no. 4, pp. 193–203, Aug. 1998.
[55] M. A. Lefsky, M. Keller, Y. Panga, P. B. de Camargod, and M. O. Hunter, "Revised method for forest canopy height estimation from geoscience laser altimeter system waveforms," *J. Appl. Remote Sens.*, vol. 1, p. 013 537, 2007.
[56] T. Herring and K. Quinn, "Atmospheric delay correction to GLASlaser altimeter ranges," Sci. Syst. Appl., Inc., Lanham, MD, 1999. GLAS Algorithm Theoretical Basis Document, Ver. 1.0, Tech. Rep.
[57] A. T. Nguyen and T. A. Herring, "Analysis of ICESat data using Kalman filter and Kriging to study height changes in East Antarctica," *Geophys. Res. Lett.*, vol. 32, no. 23, pp. L23 S03.1–L23 S03.4, Dec. 2005.
[58] J. W. Muller, "Possible advantages of a robust evaluation of comparisons," *J. Res. Nat. Inst. Standards Technol.*, vol. 105, no. 4, pp. 551–555, Jul./Aug. 2000.
[59] T. Urban, R. Gutierrez, and B. Schutz, "Analysis of ICESat laser altimetry elevations over ocean surfaces: Sea state and cloud effects," in *Proc. IEEE IGARSS*, Boston, MA, Jul. 6–11, 2008.

Hieu Duong (S'06–A'08) received the B.E degree in electrical and electronic engineering from Ho Chi Minh City University of Technology, Ho Chi Minh City, Vietnam, in 1999 and the M.Eng. degree in remote sensing and GIS from the Asian Institute of Technology, Bangkok, Thailand, in 2003. He is currently working toward the Ph.D. degree in optical and laser remote sensing, and mathematical geodesy and positioning from the Delft University of Technology, Delft, The Netherlands. His thesis topic is "Large Footprint Full Waveform Analysis in Laser Scanning Data and Applications."

Roderik Lindenbergh received the M.S. degree in mathematics from the University of Amsterdam, Amsterdam, The Netherlands, in 1994 and the Ph.D. degree in mathematics from Utrecht University, Utrecht, The Netherlands, in 2002.

He was a Scientific Programmer with the Research Institute for Applications of Computer Algebra, Eindhoven, The Netherlands, in 1995 and a Research Assistant in computational group theory with Queen Mary and Westfield College, London, U.K., in 1996. In 2002, he joined the Delft Institute of Earth Observation and Space Systems, Delft University of Technology, where he is currently an Assistant Professor in the Chair of Optical and Laser Remote Sensing. His recent work includes deformation analysis and quality aspects of remote sensing and surveying data, with emphasis on the analysis of laser ranging data from both terrestrial laser scanners and airborne and satellite platforms (ICESat) and fusion of integrated water vapor observations from GPS ground stations and the MERIS spectrometer.

Norbert Pfeifer received the Dipl.Ing. and Dr. degrees in surveying engineering from the Vienna University of Technology, Vienna, Austria, in 1997 and 2002, respectively.

He was an Assistant Professor with the Delft University of Technology and a Senior Researcher with the alp-S, Centre of Natural Hazard Management, Innsbruck, Austria. He is currently a Professor of photogrammetry with the Institute of Photogrammetry and Remote Sensing, Vienna University of Technology. His research interests include topographic and 3-D modeling, laser scanning, and automatic scene reconstruction.

Prof. Pfeifer is a member of the International Society of Photogrammetry and Remote Sensing.

George Vosselman received the M.Sc. degree in geodetic engineering from the Delft University of Technology, Delft, The Netherlands, in 1986 and the Ph.D. degree from the University of Bonn, Bonn, Germany, in 1991.

From 1993 to 2004, he was a Professor of photogrammetry and remote sensing with the Delft University of Technology. Since 2004, he has been a Professor of geo-information extraction with sensor systems with the International Institute for Geo-Information Science and Earth Observation (ITC), Enschede, The Netherlands. Since 2005, he has been the Editor-in-Chief for the *ISPRS Journal of Photogrammetry and Remote Sensing*. He has been chair or co-chair of three ISPRS working groups on processing point clouds since 2000. His research interests include methods for semiautomated and automated mapping using imagery and point clouds, and the quality analysis of data acquired with laser scanners.

Prof. Vosselman was the recipient of the ISPRS Otto von Gruber Award and the Hansa Luftbild Award.